Supporting Information

3D Printable Modular Soft Elastomers from Physically Crosslinked Homogeneous Associative Polymers

Myoeum Kim[1, †], Shifeng Nian[1, †], Daniel A. Rau[1, †], Baiqiang Huang[1], Jinchang Zhu[1], Guillaume Freychet[4], Mikhail Zhernenkov[4], Li-Heng Cai[1,2,3,*]

[1]Soft Biomatter Laboratory, Department of Material Science and Engineering, University of Virginia, Charlottesville, VA 22904, USA

[2]Department of Chemical Engineering, University of Virginia, Charlottesville, VA 22904, USA

[3]Department of Biomedical Engineering, University of Virginia, Charlottesville, VA 22904, USA

[4]National Synchrotron Light Source-II, Brookhaven National Laboratory, Upton, NY 11973, USA

* Corresponding author. Email: liheng.cai@virginia.edu; ORCID: 0000-0002-6806-0566

[†]Equal contribution

Corresponding author contact:
Dr. Li-Heng Cai
228 Wilsdorf Hall
University of Virginia
395 McCormick Road
Charlottesville, VA 22904
Tel: 434-924-2512
Fax: 434-982-5660

Table of Contents

SI Materials and Methods

Polymer synthesis and characterization. The synthesis of a linear-associative-linear (LAL) triblock copolymer consists of two steps: (1) the reversible middle block, and then (2) using the middle block as a macro-initiator to grow the two end linear blocks. For both steps, we use activator regenerated by electron transfer (ARGET) atom transfer radical polymerization (ATRP).[1] We synthesize the reversible block by copolymerizing hexyl acrylate (HA) with 5-acetamidopentyl acrylate (AAPA), which carries an amide group at one of its two ends and serves as the sticky monomer. The reaction conditions for the synthesis are summarized in **Table S1**. Below we describe the detailed synthesis protocols.

Step I. Synthesis of sticky monomer 5-acetamido pentyl acrylate (AAPA). AAPA is synthesized based on previously described methods.[2,3] First, a flask is charged with 5-amino-1-pentanol (25 g, 242.3 mmol) and ethyl acetate (250 mL). Acetic anhydride (28.1 g, 275.4 mmol) is added dropwise with vigorous stirring under nitrogen. After finishing the addition of acetic anhydride, the reaction mixture is stirred at room temperature for 2 hours followed by the addition of methanol (80 mL) and K_2CO_3 (28 g, 202.6 mmol). The mixture is vigorously stirred for another 15 min followed by the filtration of undissolved solid if any. The filtered solution is concentrated by a rotary evaporator (Buchi R-205) to obtain 5-acetamido-1- pentanol (AAPA, 30.5 g) with a yield of 87.1%. The success for the synthesis of AAPA is confirmed by ^{1}H NMR (600 MHz, $CDCl_3$) δ=3.53 (t, 2H), 3.14 (q, 2H), 1.89 (s, 3H), 1.47 (m, 4H), 1.32 (m, 4H).

Second, a flask is charged with 5-acetamido-1- pentanol (3.34 g, 23.0 mmol), acrylic acid (2.48 g, 34.5 mmol), EDC (7.27 g, 37.9 mmol), *N*,*N*-diisopropylethylamine (4.9 g, 37.9 mmol) and dichloromethane (100 mL). The reaction is stirred at room temperature for 48 h under nitrogen. Then the reaction mixture is diluted with another 100 mL dichloromethane. Then the solution is sequentially washed with aqueous solutions of NaOH (1.0 M, 100 mL), aqueous solution of HCl (1.0 M, 100 mL), saturated aqueous solutions of $NaHCO_3$ (150 mL) and saturated aqueous solution of NaCl (150 mL) The organic supernatant is dried with Na_2SO_4 for 12 h and then concentrated by a rotary evaporator to obtain the crude product. The crude product is purified by passing through a silica column using ethyl acetate/hexanes = 1/9 (v/v) as eluent. 5-acetamido pentyl acrylate (AAPA) (3.6 g) is obtained with a yield of 78.6%. ^{1}H NMR (600 MHz, $CDCl_3$) δ=6.37 (d, 1H),

6.11 (dd, 1H), 5.82 (d, 1H), 5.58 (s, 1H), 4.15 (t, 2H), 3.23 (q, 2H), 1.96 (s, 3H), 1.68 (m, 2H), 1.53 (m, 2H), 1.39 (m, 2H).

Step II-a. Synthesis of control middle block poly(hexyl acrylate) (PHA). A 25 mL Schlenk flask is charged with 2f-BiB (23 mg, 0.064 mmol), HA (5 g, 32.0 mmol) and anisole (6 mL). We dissolve Me_6TREN (92 mg, 0.4 mmol) and $CuCl_2$ (5.4 mg, 0.04 mmol) in 1 mL DMF to make a catalyst solution. Then, we add 160 μL catalyst solution, containing 6.4×10^{-2} mmol Me_6TREN and 6.4×10^{-3} mmol $CuCl_2$, to the mixture and bubble it with nitrogen for 30 min to remove oxygen. Afterward, the reducing agent, $Sn(EH)_2$ (52 mg, 0.128 mmol) in 200 μL anisole, is quickly added to the reaction mixture using a glass pipet. We seal the flask and then immerse it in an oil bath at 70°C to start the reaction. We monitor the reaction by taking out a small amount of mixture every 30 mins to determine the conversion using proton NMR and stopped the reaction after 126 min. Based on ^{1}H NMR, the conversion is 50.2% and the degree of polymerization (DP) is 251.

The rest of the reaction mixture is diluted with THF and passed through a neutral aluminum oxide column to remove the catalyst. The collected solution is concentrated by a rotary evaporator. We use methanol to precipitate the polymer, re-dissolve the sediment in THF to make a homogenous solution and repeat this precipitation procedure another 2 times to ensure that all unreacted monomers and impurities are completely removed. After purification, the sample is dissolved in THF and transferred to a glass vial and dried in the hood for 16 h, then transferred to a vacuum oven (Thermo Fisher, Model 6258) at room temperature for 24 h to completely remove the solvent.

Step II-b. Synthesis of reversible middle block with 8.8% of sticky monomers. A 25 mL Schlenk flask is charged with 2f-BiB (22.4 mg, 0.062 mmol), HA (4.38 g, 28.0 mmol), AAPA (0.62 g, 3.11 mmol) and anisole (6 mL). We dissolve Me_6TREN (92 mg, 0.4 mmol) and $CuCl_2$ (5.4 mg, 0.04 mmol) in 1 mL DMF to make a catalyst solution. Then, we add 155 μL catalyst solution, containing 6.2×10^{-2} mmol Me_6TREN and 6.2×10^{-3} mmol $CuCl_2$, to the mixture and bubble it with nitrogen for 30 min to remove oxygen. Afterwards, the reducing agent, $Sn(EH)_2$ (50.4 mg, 0.125 mmol) in 200 μL anisole, is quickly added to the reaction mixture using a glass pipet. We seal the flask and then immerse it in an oil bath at 80°C to start the reaction. The reaction is monitored by taking out a small amount of mixture to determine the conversion using proton NMR and stopped after 109

min. From proton NMR, the conversion is 52.4% and the total degree of polymerization (DP) is 262. The purification procedure is the same as the synthesis of controlled middle block. After purification, from ^{1}H NMR, the DP of HA is 239, the DP of AAPA is 23, the ratio of reversible bond is 8.8%.

Step II-c. Example of the synthesis of the reversible middle block with 25% of sticky monomers. A 25 mL Schlenk flask is charged with 2f-BiB (21.5 mg, 0.060 mmol), HA (3.5 g, 22.4 mmol), AAPA (1.5 g, 7.53 mmol) and anisole (6 mL). We dissolve Me_6TREN (92 mg, 0.4 mmol) and $CuCl_2$ (5.4 mg, 0.04 mmol) in 1 mL DMF to make a catalyst solution. Then, we add 150 μL catalyst solution, containing 6.0×10^{-2} mmol Me_6TREN and 6.0×10^{-3} mmol $CuCl_2$, to the mixture and bubble it with nitrogen for 30 min to remove oxygen. Afterwards, the reducing agent, $Sn(EH)_2$ (48.4 mg, 0.12 mmol) in 200 μL anisole, is quickly added to the reaction mixture using a glass pipet. We seal the flask and then immerse it in an oil bath at 80°C to start the reaction. The reaction is monitored by taking out a small amount of mixture to determine the conversion using ^{1}H NMR and stopped after 100 min. From ^{1}H NMR, the conversion is 48.0% and the DP is 240. The purification procedure is similar to the synthesis of the control middle block. The only difference is that a co-solvent is used for precipitation; the co-solvent is a mixture of hexanes and diethyl ether with a volume ratio 3:1, which is a good solvent for both HA and AAPA but not for the reversible middle block. After purification, from ^{1}H NMR, the DP of HA is 180, the DP of AAPA is 60, and the percentage of sticky monomers is 25% or $\lambda = 0.25$.

Step III-a. Synthesis of the control triblock copolymer PBnMA-PHA-PBnMA. A 25 mL Schlenk flask is charged with benzyl methacrylate (BnMA, 705 mg, 4 mmol), macroinitiator (40 kg/mol, 800 mg, 0.02 mmol) and anisole (4 mL). We dissolve Me_6TREN (92 mg, 0.4 mmol) and $CuCl_2$ (5.4 mg, 0.04 mmol) in 1 mL DMF to make a catalyst solution. We add 40 μL catalyst solution, containing 1.6×10^{-2} mmol Me_6TREN and 1.6×10^{-3} mmol $CuCl_2$, to the mixture and bubble it with nitrogen for 30 min to remove oxygen. Afterwards, reducing agent, $Sn(EH)_2$ (25.9 mg, 0.064 mmol) in 150 μL anisole, is quickly added to the reaction mixture using a glass syringe. Then, we seal the flask and immerse it in an oil bath at 60°C. The reaction is monitored by taking out a small amount of mixture to determine the DP of PBnMA using ^{1}H NMR. The reaction is stopped after 120 min. The reaction mixture is diluted in THF and passed through a neutral aluminum oxide

column to remove the catalyst, and the collected solution is concentrated by a rotavapor. We use methanol for precipitation three times; this completely removes all unreacted monomers and impurities. After purification, the sample is dissolved in dichloromethane and transferred to a glass vial and dried in the hood for 16 h, then the vial is put in a vacuum oven at room temperature for 24 h to completely remove the solvent. After purification, from ^{1}H NMR, the DP of PBnMA on each end is 15.

Step III-b. Synthesis of LAL triblock copolymers with 8.8% of sticky monomers in the middle block. A 25 mL Schlenk flask is charged with BnMA (583 mg, 3.31 mmol), macroinitiator (42 kg/mol, 700 mg, 0.017 mmol) and anisole (3.3 mL). We dissolve Me_6TREN (92 mg, 0.4 mmol) and $CuCl_2$ (5.4 mg, 0.04 mmol) in 1 mL DMF to make a catalyst solution. We add 33 μL catalyst solution, containing 1.3×10^{-2} mmol Me_6TREN and 1.3×10^{-3} mmol $CuCl_2$, to the mixture and bubble it with nitrogen for 30 min to remove oxygen. Afterwards, reducing agent, $Sn(EH)_2$ (21.5 mg, 0.053 mmol) in 150 μL anisole, is quickly added to the reaction mixture using a glass syringe. Then, we seal the flask and immerse it in an oil bath at 60°C. The reaction is monitored by taking out a small amount of mixture to determine the DP of PBnMA using proton NMR. The reaction is stopped after 103 min. The purification procedure is the same as the synthesis of controlled triblock copolymer. After purification, from ^{1}H NMR, the DP of PBnMA on each end is 18.

Step III-c. Example of synthesis of LAL triblock copolymers with 25% of sticky monomers in middle block. A 25 mL Schlenk flask is charged with BnMA (529 mg, 3 mmol), macroinitiator (40 kg/mol, 610 mg, 0.015 mmol) and anisole (3 mL). We dissolve Me_6TREN (92 mg, 0.4 mmol) and $CuCl_2$ (5.4 mg, 0.04 mmol) in 1 mL DMF to make a catalyst solution. We add 30 μL catalyst solution, containing 1.2×10^{-2} mmol Me_6TREN and 1.2×10^{-3} mmol $CuCl_2$, to the mixture and bubble it with nitrogen for 30 min to remove oxygen. Afterwards, reducing agent, $Sn(EH)_2$ (19.4 mg, 0.048 mmol) in 150 μL anisole, is quickly added to the reaction mixture using a glass syringe. Then, we seal the flask and immerse it in an oil bath at 60°C. The reaction is monitored by taking out a small amount of mixture to determine the DP of PBnMA using proton NMR. The reaction is stopped after 61 min. The purification procedure is the same as the synthesis of controlled triblock copolymer. After purification, from ^{1}H NMR, the DP of PBnMA on each end is 16.

^{1}H NMR characterization. We use ^{1}H NMR to determine the conversion of HA and AAPA and the volume fraction of PBnMA. Chemical shifts for ^{1}H NMR spectra are reported in parts per million compared to a singlet at 7.26 ppm in $CDCl_3$.

Conversion of HA monomers for the control middle block. The conversion is calculated based on the conversion of HA monomers to the polymer poly(hexyl acrylate) (PHA), which is measured by the NMR spectra of the raw reaction mixture, as shown in **Fig. S1**. The area of peak **a** at 4.18 ppm, A_{HA}, corresponds to two H on the methylene group connected with the oxygen atom in HA monomer. The area of peak **a'** at 4.08 ppm, A_{PHA}, corresponds to two H on the methylene group connected with the oxygen atom in HA repeating unit of PHA. The conversion of HA equals to $A_{PHA} \times 100\% / (A_{HA} + A_{PHA})$. For example, for the reaction in **Fig. S1**, the conversion of HA is $1.01 \times 100\% / (1 + 1.010) = 50.2\%$. Because the molar ratio between HA monomer and initiator is 500, the degree of polymerization (DP) of PHA is $500 \times 50.2\% = 251$.

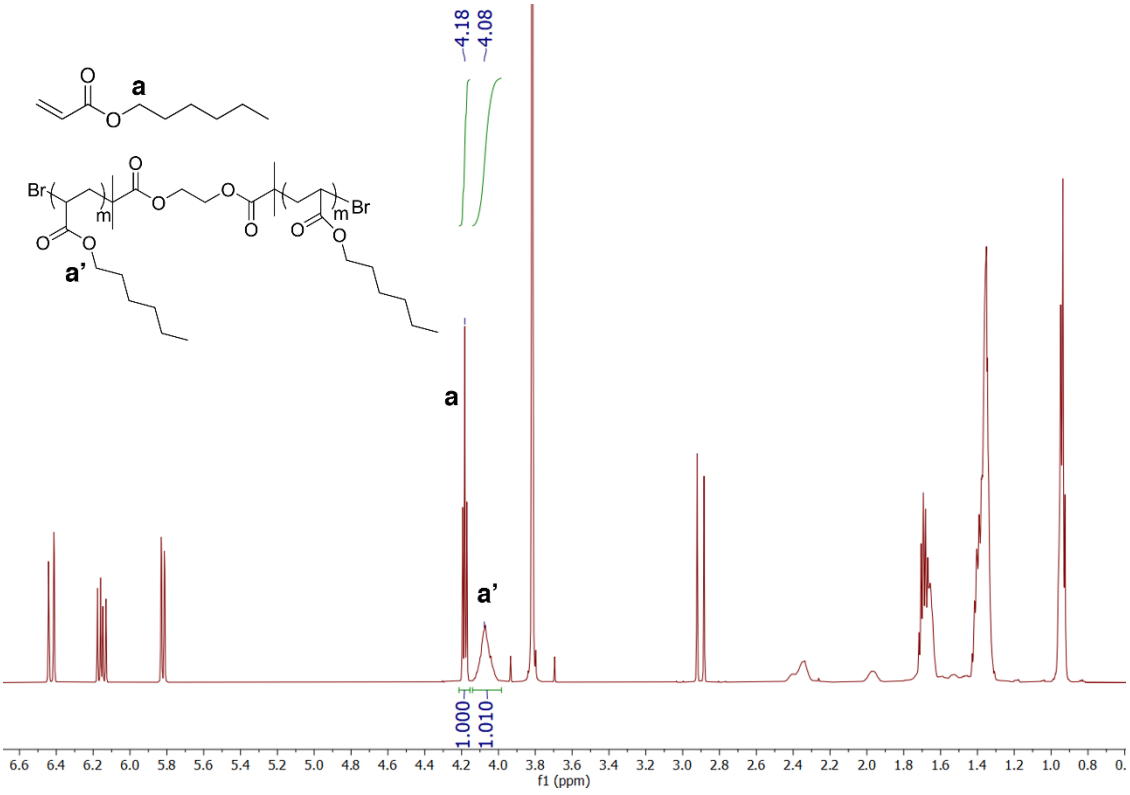

Figure S1. ^{1}H NMR spectra of raw mix of ARGET ATRP of HA.

Example of conversion of HA and AAPA for reversible middle block. The total conversion is calculated based on the conversion of HA and AAPA to the polymer poly(HA-*r*-AAPA), which is measured by the NMR spectra of the raw reaction mixture, as shown in **Fig. S2**. The area of peak **a** A_{HA} and peak **b** A_{AAPA} at 4.18 ppm corresponds to two H on the methylene group connected with the oxygen atom in HA and AAPA monomers, respectively. The area of peak **a'** A_{PHA} and **b'** A_{PAAPA} at 4.06 ppm corresponds to two H on the methylene group connected with the oxygen atom in HA and AAPA repeating units, respectively. The total conversion of HA and AAPA equals to $(A_{PHA}+A_{PAAPA})\times$ 100% / $(A_{HA}+A_{PHA}+A_{AAPA}+A_{PAAPA})$. The total conversion of HA and AAPA in **Fig. S2** equals to 1.103×100% / (1+1.103) = 52.4%. For this polymerization, the molar ratio between HA and AAPA and initiator is 500. Therefore, the total DP and P(HA-*r*-AAPA) is 500 × 52.4% = 262.

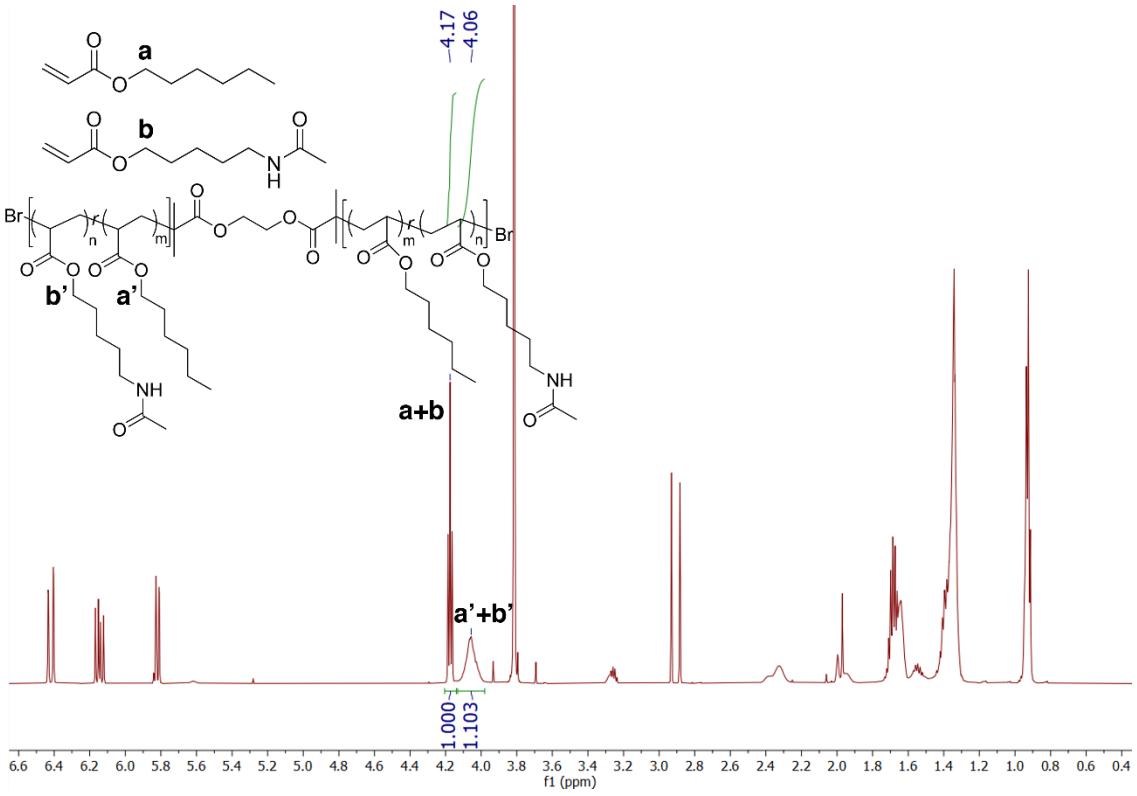

Figure S2. ^{1}H NMR spectra of raw mix of ARGET ATRP of HA and AAPA.

Example for the calculation of the fraction of reversible groups in reversible middle block. In **Fig. S3**, the area of peak **a** $A_{PHA\text{-}O}$ and peak **b** $A_{PAAPA\text{-}O}$ at 4.00 ppm corresponds to two H on the

methylene group connected with the oxygen atom in HA and AAPA repeating units, respectively. The area of peak **c** $A_{PAAPA\text{-}N}$ at 3.24 ppm corresponds to two H on the methylene group connected with the nitrogen atom in AAPA repeating units. The fraction of reversible groups equals to $A_{PAAPA\text{-}N}$ × 100% / ($A_{PHA\text{-}O}$+$A_{PAAPA\text{-}O}$). The fraction of reversible groups in **Fig. S3** equals to 0.087×100% / 1 = 8.7%. For this middle block copolymer, the total DP for P(HA-*r*-AAPA) is 262. Therefore, the DP of AAPA is 262 × 8.7% = 23, the DP of HA is 262-23 = 239.

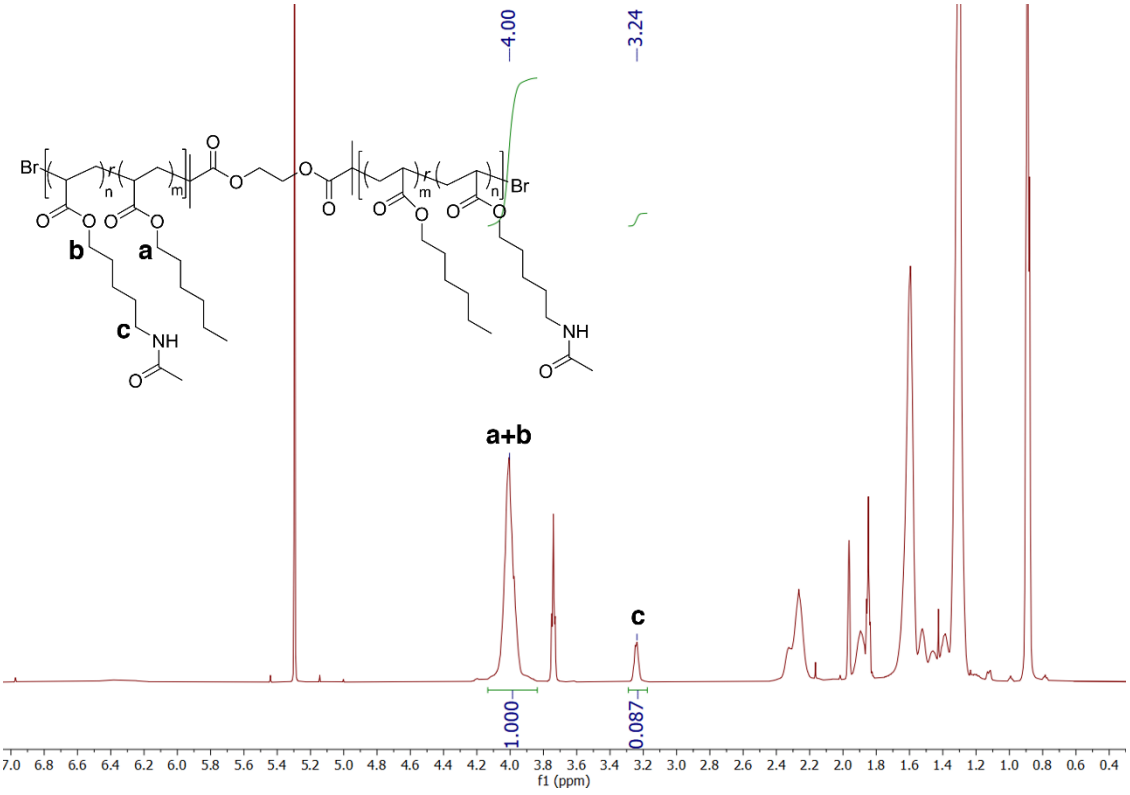

Figure S3. ^{1}H NMR spectra of reversible middle block, HA$_{239}$-*r*-AAPA$_{23}$.

Calculation of DP and volume fraction of end block PBnMA for the control triblock copolymer. The volume fraction of PBnMA is determined based on the NMR spectra of purified triblock copolymers. For example, in **Fig. S4**, the area of peak **a** at 4.86 ppm, A_{PBnMA}, corresponds to the two H on the methylene group of BnMA repeating unit of PBnMA. The area of peak at 4.01 ppm, A_{PHA}, corresponds to two H on the methylene group connected with the oxygen atom in HA repeating unit of PHA. Therefore, the DP of PBnMA is $n_{BnMA} = n_{HA} \times (A_{PBnMA}/2)/(A_{PHA}/2) = 30$, in which $A_{BnMA} = 0.121$, $A_{PHA} = 1.000$, and the DP of PHA is $n_{HA} = 251$. The volume fraction of PBnMA is given by $f = (n_{BnMA} \times m_{BnMA}/d_{PBnMA})/ (n_{BnMA} \times m_{BnMA}/d_{PBnMA} + n_{HA} \times m_{HA}/d_{PHA}) \times 100\% =$ 10.4%, in which the density of PBnMA is 1.179 g/mL, the density of PHA is 1.04 g/mL, the mass of a BnMA monomer $m_{BnMA} = 176.21$ g/mol, and that of a HA monomer $m_{HA} = 156.23$ g/mol.

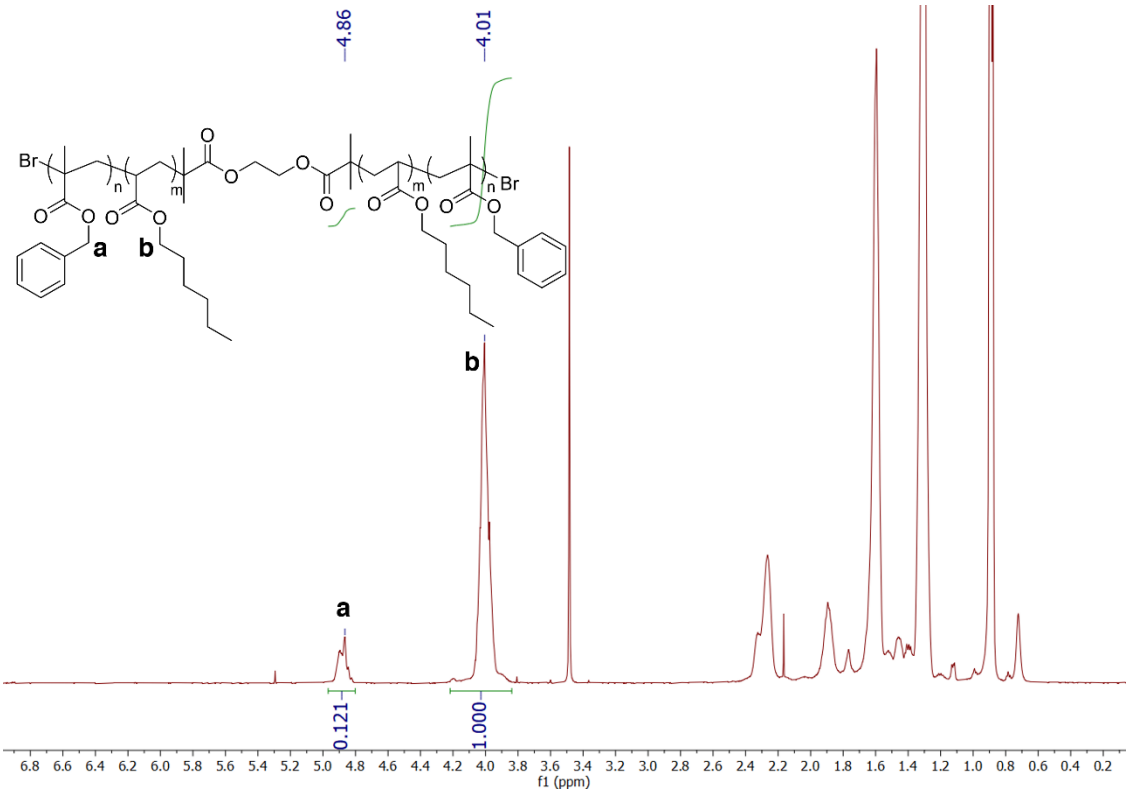

Figure S4. ^{1}H NMR spectra of sample TR1, BnMA$_{15}$-*b*-HA$_{251}$-*b*-PBnMA$_{15}$.

Example of calculation of DP and volume fraction of end block PBnMA for reversible triblock copolymers. The volume fraction of PBnMA is determined based on the NMR spectra of purified triblock copolymers. For example, in **Fig. S5**, area of peak **c** at 4.87 ppm is A_{PBnMA}, corresponding to the two H on the methylene group of BnMA repeating unit. Area of peak at 4.01 ppm is the total area **a** A_{PHA} and **b** A_{PAAPA}, corresponds to two H on the methylene group connected with the oxygen atom in HA and AAPA repeating units, respectively. Therefore, the degree of polymerization of PBnMA is $n_{BnMA} = n_{HA} \times (A_{PBnMA}/2)/((A_{PHA} + A_{PAAPA})/2) = 36$, in which $A_{BnMA} = 0.139$, $A_{PHA} + A_{PAAPA} = 1.000$, and the DP of HA is $n_{HA} = 239$, DP of AAPA is $n_{AAPA} = 23$. The volume fraction of PBnMA is given by $f = (n_{BnMA} \times m_{BnMA}/d_{PBnMA})/(n_{BnMA} \times m_{BnMA}/d_{PBnMA} + n_{HA} \times m_{HA}/d_{PHA} + n_{AAPA} \times m_{AAPA}/d_{PAAPA}) \times 100\% = 11.5\%$, in which the density of PBnMA is 1.179 g/mL, the density of PHA and PAAPA is 1.04 g/mL, the mass of a BnMA monomer $m_{BnMA} = 176.21$ g/mol, the mass of a HA monomer $m_{HA} = 156.23$ g/mol and the mass of a AAPA monomer $m_{HA} = 199.25$ g/mol.

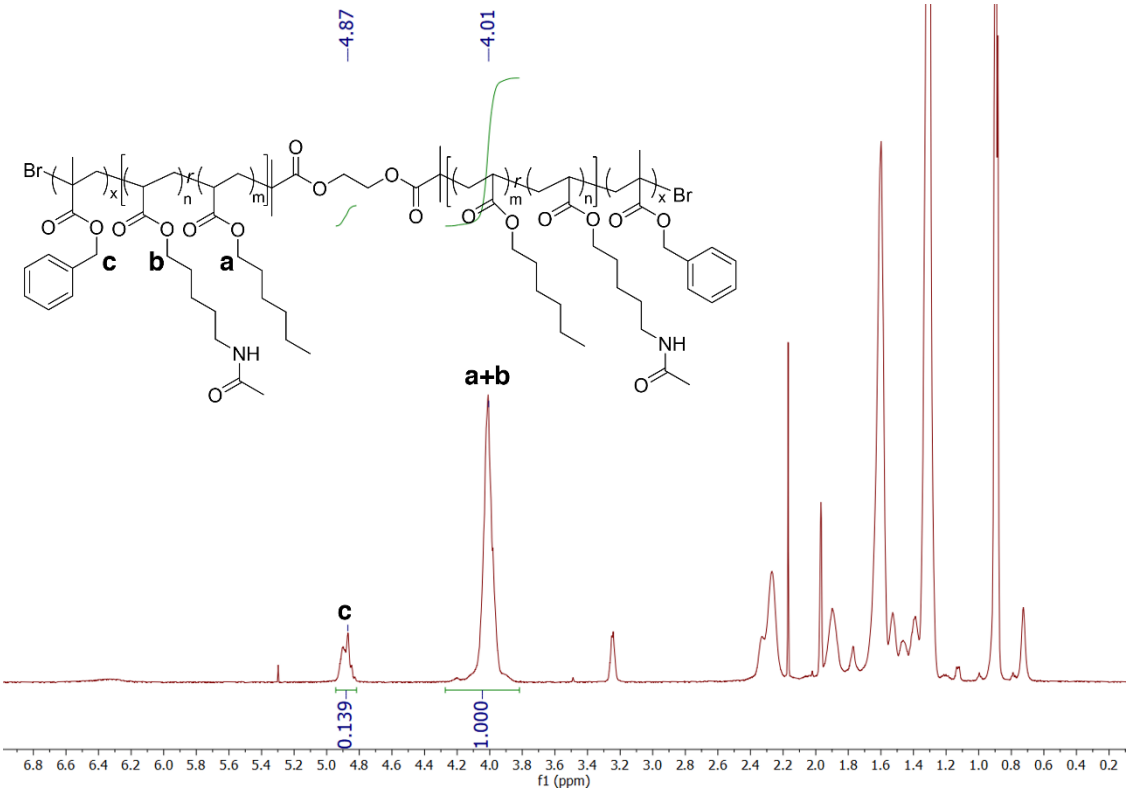

Figure S5. ^{1}H NMR spectra of sample TR2, BnMA$_{18}$-*b*-(HA$_{239}$-*r*-AAPA$_{23}$)-*b*-PBnMA$_{18}$.

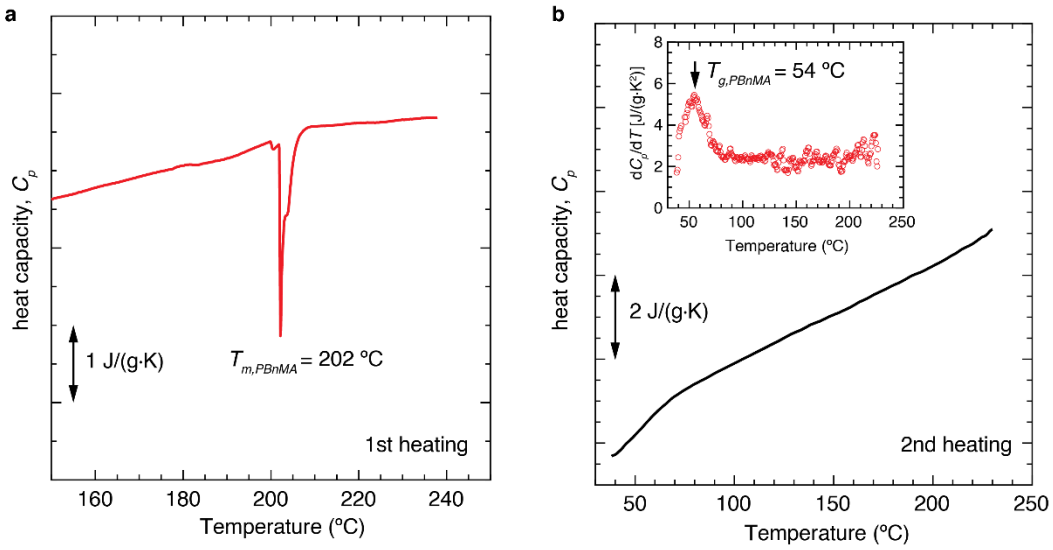

Figure S6. Dependence of heat capacity, C_p, of the LAL polymer with λ=0.25 and f=31% measured by differential scanning calorimetry.

In the self-assembled network, **(a)** the melting of the PBnMA is 202 ℃, and **(b)** the glass transition temperature of PBnMA is 54 ℃.

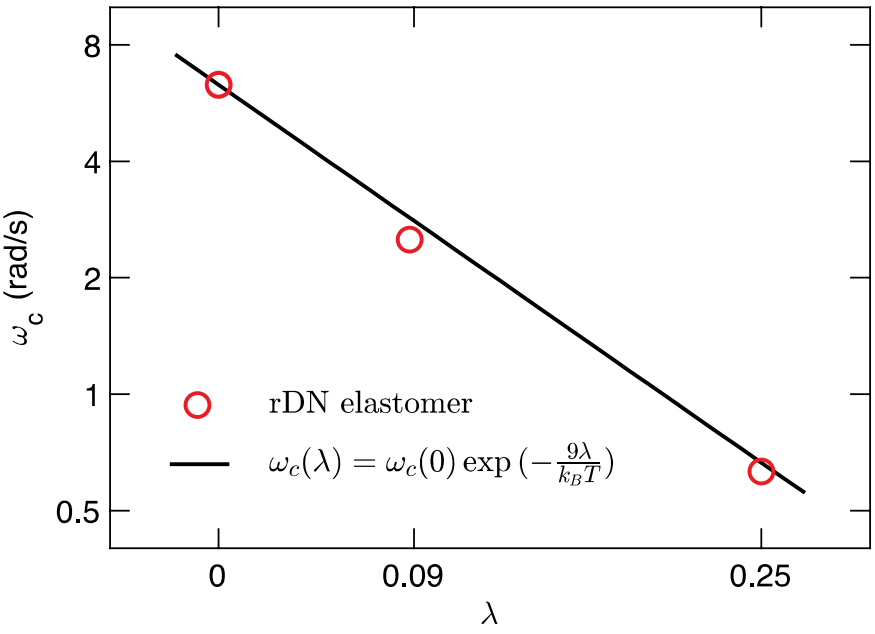

Figure S7. Dependence of crossover frequency on fraction of associative group for LAL polymers with *f* around 11%.

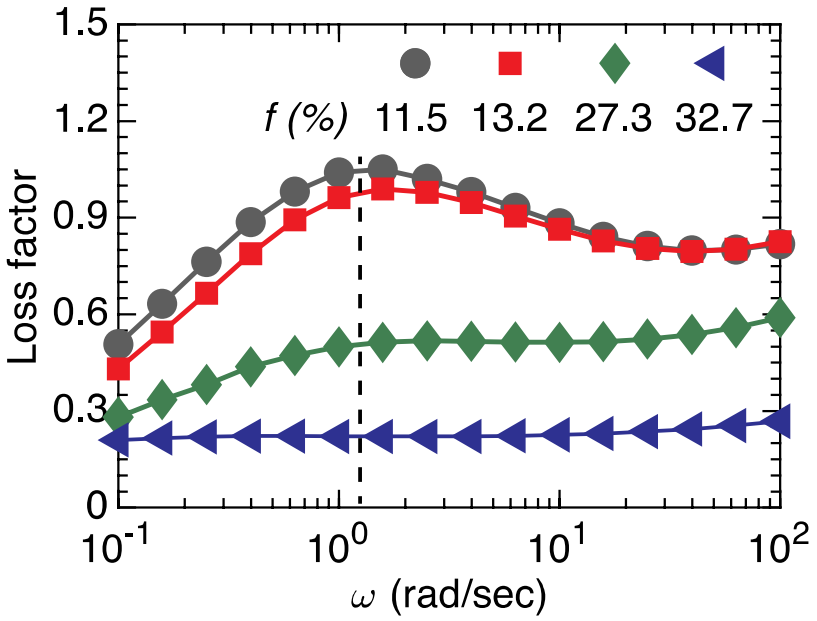

Figure S8. Relationship between loss factor and frequency.

LAL polymers with $\lambda = 0.25$ and different f. Dashed line indicates the frequency associated with the peak of the loss factor, which is determined by the fraction of reversible bonds and thus a constant regardless of the volume fraction of the end blocks.

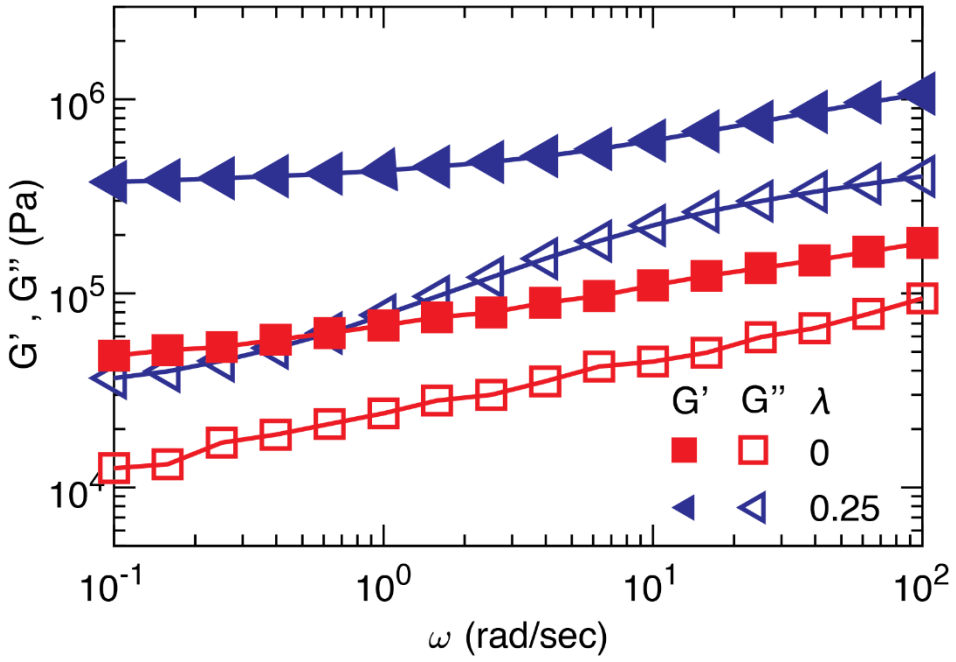

Figure S9. Frequency dependence of shear moduli of LAL polymers for printing.

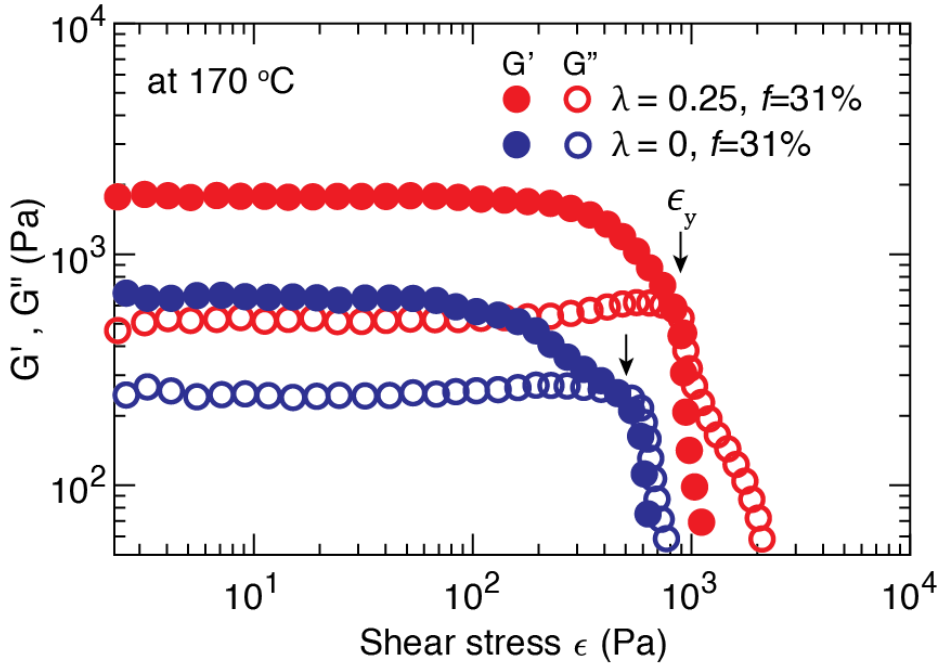

Figure S10. Yield-stress behavior of LAL polymer at 170 ℃.

The stress sweep reveals a yielding at a critical stress (ϵ_y) defined as the crossover of *G'* and *G"*. The measurement is performed at a fixed oscillatory frequency of 1 rad/sec with increasing shear stress.

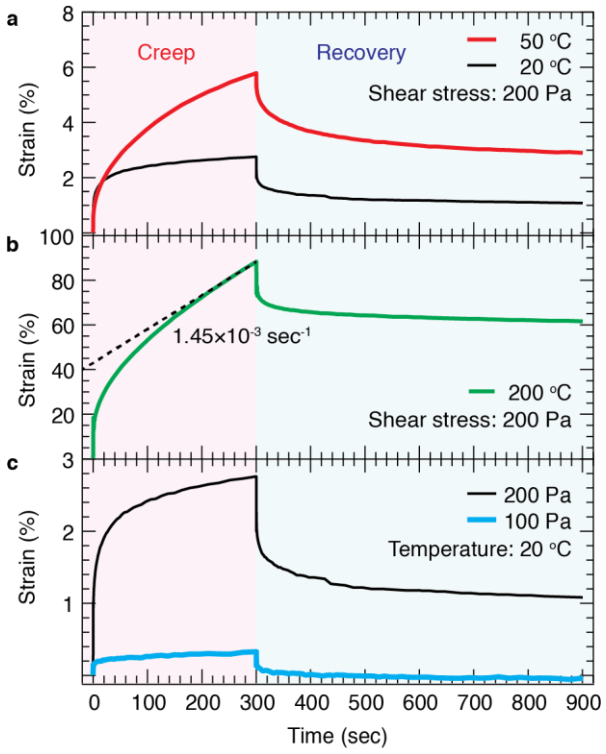

Figure S11. Creep-recovery measurements of LAL polymer with=0.25 and *f*=31%.

(a, b) The polymer is applied by a constant shear stress of 200 Pa at various temperatures. **(c)** The polymer is applied to different shear stresses at 20 °C.

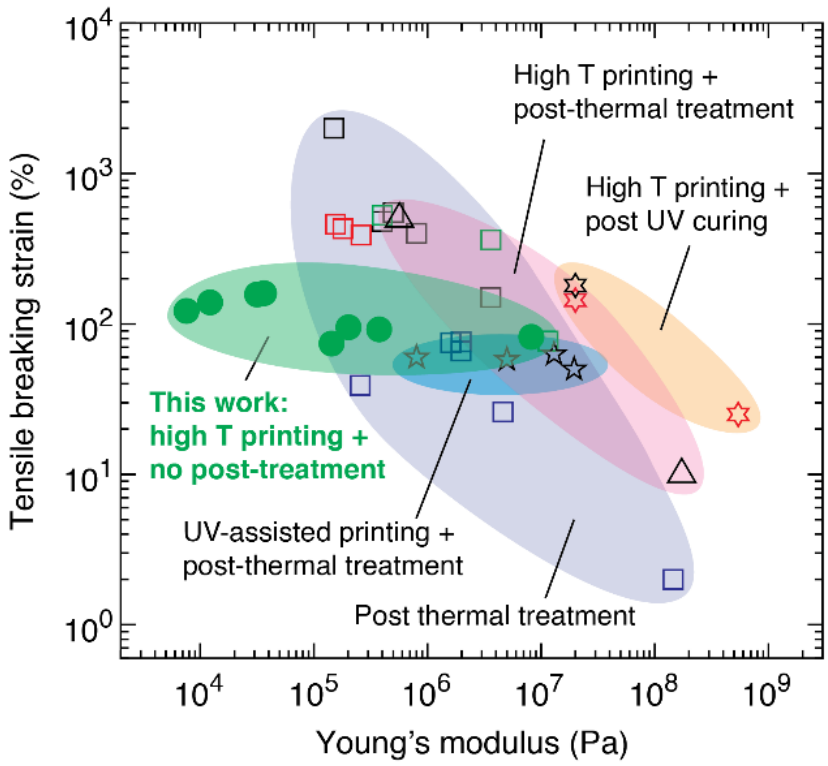

Figure S12. Ashby-type plot comparing LAL polymers to solvent-free and DIW printable polymer composites.

The mechanical properties are based on tensile breaking strain and Young's modulus. Closed circles: our modular soft elastomers for DIW printing; other symbols: literature data (**Table S4**).

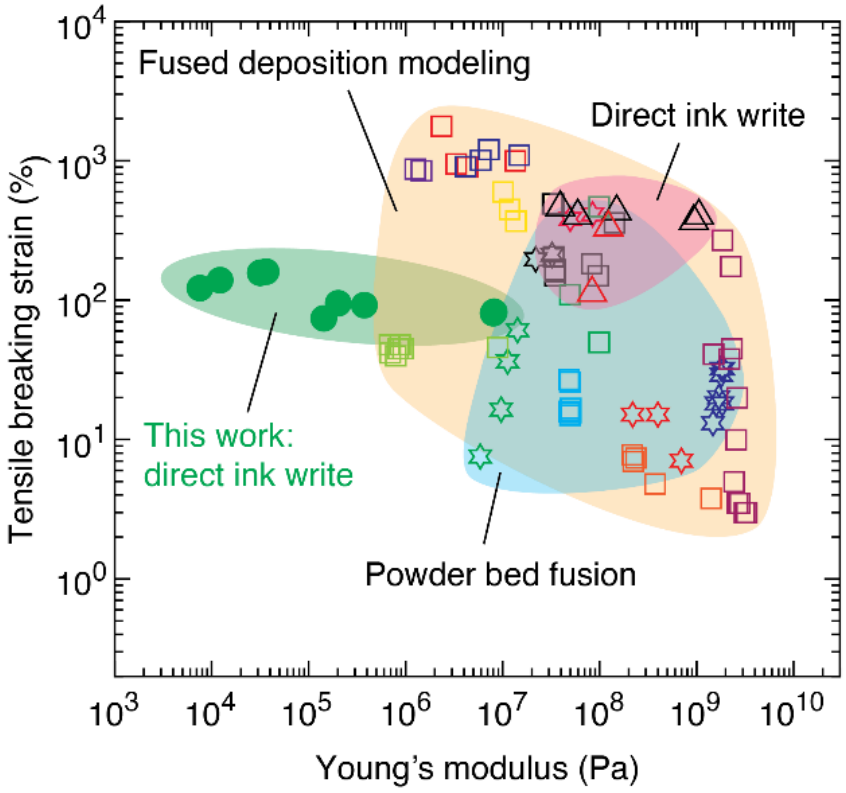

Figure S13. Ashby-type plot of thermoplastic polymers for different additive manufacturing techniques.

The mechanical properties are based on tensile breaking strain and Young's modulus. Closed circles: our modular soft elastomers for DIW printing; other symbols: literature data (**Table S5**).

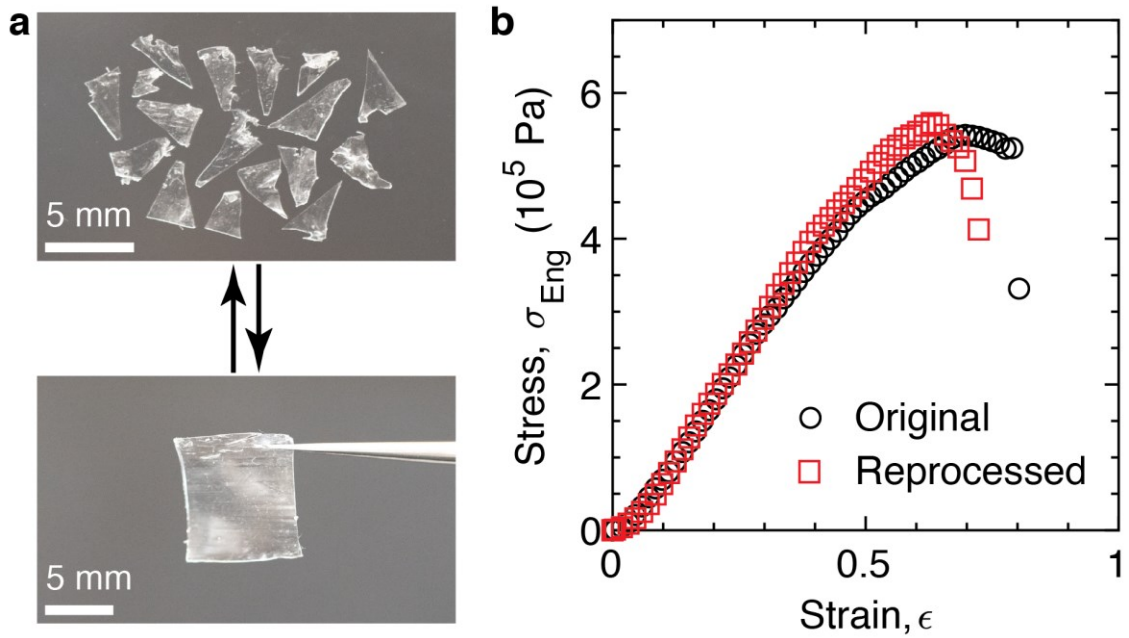

Figure S14. The self-assembled polymer networks are reprocessable.

(**a**) Optical images of a chopped polymer (sample TV2; upper) and that reprocessed using solvent (dichloromethane) (lower). (**b**) Stress-strain curves of the original (circles) and the reprocessed (squares) polymers under uniaxial tensile tests at a fixed strain rate of 0.01/sec.

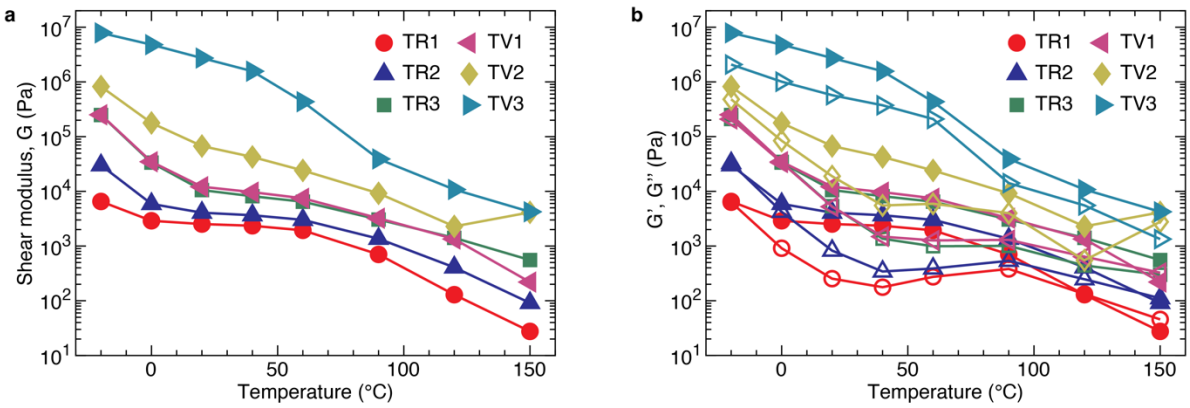

Figure S15. Dependence of modulus of LAL polymers on temperature.

(a) Dependence of shear modulus (*G'* at 0.1 rad/sec and 0.5% strain) on temperature. **(b)** Dependencies of both storage (filled symbols) and loss (empty symbols) moduli on temperature. All measurements are performed at a fixed oscillatory shear strain of 0.5% and frequency of 1 rad/sec.

Table S1. Summary of synthesis conditions of all middle block and triblock polymers.

(1) Catalyst is made by dissolving Me_6TREN (92 mg, 0.4 mmol) and $CuCl_2$ (5.4 mg, 0.04 mmol) in 1 mL DMF. (2) The reaction temperature is 80 °C for all middle block polymers and is 60 °C for all triblock polymers.

Sample	Middle block								Triblock					
	HA (mmol)	AAPA (mmol)	Initiator (mmol)	Catalyst (μL)	$Sn(EH)_2$ (mmol)	Anisole (mL)	Time (min)	Conv. (%)	BnMA (mmol)	Macro-initiator (mmol)	Catalyst (μL)	$Sn(EH)_2$ (mmol)	Anisole (mL)	Time (min)
TV1	32	0	0.064	160	0.128	6	126	50.2	4	0.020	40	0.064	4	120
TV2	28	3.11	0.062	156	0.125	6	109	52.4	3.31	0.017	33	0.053	3.3	103
TV3	22.4	7.53	0.060	150	0.119	6	100	48.0	3	0.015	30	0.048	3	61
TR1									3.46	0.017	20	0.020	3.5	183
TR2	22.4	7.53	0.060	150	0.119	6	133	50	4.35	0.014	44	0.070	4.5	166
TR3									4.65	0.015	47	0.074	4.7	190

Table S2. List of data points and references for Fig. 5d.

Printing Method	Symbol Shape	Materials	Symbol color	Young's modulus (kPa)	Tensile strain (%)	Reference number
Post UV curing	Diamond (◊)	Polydimethylsiloxane (PDMS)	Black	94	385	Yirmibeseglu et al.[4]
				90	295	
				85	350	
				84	270	
				80	260	
		Acrylic polymer	Red	5,909	55	Su et al.[5]
				2,000	90	
				1,200	110	
				1,000	120	
				500	150	
				94	317	
		Bottle brush polymers	Green	25.8	200	Xie et al.[6]
				23.1	310	
High T printing + post UV curing	Hexagram (✡)	Liquid crystal elastomer (LCE)	Black	40,000	70	Volpe et al.[7]
				13,300	120	
				6,670	420	
				700	230	
				400	470	
				100	240	
			Red	40,000	20	Kim et al.[8]
				32,630	19	
				8,000	180	
				5,000	190	
			Green	1,500	66	Wang et al.[9]
				750	80	
				400	88	
				400	82	
			Blue	10,000	70	Ambulo et al.[10]
				500	115	
				500	90	
High T printing + post-thermal treatment	Triangle (△)	LCE	Black	1,000	280	Davidson et al.[11]
				500	320	

Table S3. Molecular parameters and mechanical properties of LAL polymers for 3D printing

Samples	Processing methods	Tensile strain	Tensile strength (kPa)	Toughness (kJ/m^3)
$\lambda = 0.25, f = 0.31$	Printed	1.25	1,190	939
$\lambda = 0.25, f = 0.31$	Molded (Cast)	0.92	1,186	872
$\lambda = 0, f = 0.31$	Printed	1.15	239	132
$\lambda = 0, f = 0.31$	Molded (Cast)	0.74	368	227

Table S4. List of data points and references for Fig. S12.

Printing Method	Symbol Shape	Materials	Symbol color	Young's modulus (kPa)	Tensile strain (%)	Reference number
Post thermal treatment	Square (□)	PDMS + silica composites	Black	3,600	150	Zhou et al.[12]
				500	550	
				400	480	
				800	400	
				150	2,000	
			Blue	145,000	2	Ford et al.[13]
				4,615	26	
				1,974	76	
				1,970	66	
				1,600	75	
				256	39	
			Green	11,510	77	Durban et al.[14]
				3,610	362	
				400	528	
		PDMS + PTFE composites	Red	260	390	Zheng et al.[15]
				180	430	
				155	460	
High T printing + post UV curing	Hexagram (✡)	LCE + Liquid metal composites	Black	20,000	180	Kotikian et al.[16]
		Polycarbonate + graphite composites	Red	20,000	144	Brook et al.[17]
				542,000	25	
High T printing + post-thermal treatment	Triangle (△)	Fiber reinforced PDMS composites	Black	172,500	10	Liu et al.[18]
				566	500	
UV-assisted printing+ post-thermal treatment	Pentagram (☆)	Epoxy and acrylic polymer + silica composites	Black	19,500	50	Chen et al.[19]
				13,000	63	
				5,000	58	
				800	60	

Table S5. List of data points and references for Fig. S13.

Printing Method	Symbol Shape	Materials	Symbol color	Young's modulus (kPa)	Tensile strain (%)	Reference number
Fused Deposition Modeling (FDM)	Square (□)	Thermoplastic polyurethane (TPU)	Black	34,000	206	Georgopoulos et al.[20]
				35,000	150	
				33,000	493	
				35,000	166	
				35,000	161	
				34,000	494	
				84,000	183	
				98,000	150	
				144,000	360	
			Red	2,370	1777	Shin et al.[21]
				4,400	905	
				3,360	952	
				13,700	1003	
			Blue	4,200	912.8	Shin et al.[22]
				6,000	1013.2	
				7,300	1206.7	
				15,000	1099.8	
		Styrene ethylene butylene styrene (SEBS)	Green	100	470	Georgopoulos et al.[23]
				100	50	
				50	110	
			Purple	1,470	850	Khondoker et al.[24]
				1,270	875	
		TPU/ polylactic acid (PLA)	Magenta	3,329,000	3	Wang et al.[25]
				3,152,000	3	
				2,674,000	3.5	
				2,650,000	20	
				2,828,000	3.5	
				2,465,000	5	
				2,342,000	45	
				2,589,000	10	
				2,203,000	38	
				1,871,000	270	
				2,280,000	175	
				1,517,000	41	
		Polyhydroxy urethanes (PHUs)	Orange	220,000	7.8	Schimpf et al.[26]
				240,000	7.4	
				225,000	7.0	
				378,000	4.83	
				1,430,000	3.8	
				700,000	7	

Table S5. List of data points and references for Fig. S13 (continued).

Printing Method	Symbol Shape	Materials	Symbol color	Young's modulus (kPa)	Tensile strain (%)	Reference number
Fused Deposition Modeling (FDM)	Square (□)	Polycaprolactone (PCL)	Light blue	50,000	15	Joe et al.[27]
				50,000	26	
				51,000	15.7	
				51,000	16.8	
				49,000	16	
				49,000	27	
		Polyurea	Light green	890	48	Niu et al.[28]
				950	45	
				850	45	
				700	42	
				690	48	
				800	40	
				9,000	46	
		Ethylene-vinyl acetate (EVA)	Yellow	10,220	600	Kumar et al.[29]
				11,930	450	
				13,860	370	
Direct-ink Writing (DIW)	Triangle (△)	TPU/PCL	Black	40,330	470	Ravichandran et al.[30]
				61,060	410	
				961,530	375	
				1,084,280	410	
				153,860	440	
			Red	126,300	338.5	Ravichandran et al.[31]
				85,750	114.67	
Powder bed fusion (PBF)	Hexagram (✡)	TPU	Black	22,000	195	Hupfeld et al.[32]
				32,500	210	
			Red	50,000	380	Do et al.[33]
				85,000	410	
				220,000	15	
				400,000	15	
				700,000	7	
		Polyamide	Blue	1,480,000	13	Chen et al.[34]
				1,600,000	18	
				1,700,000	20	
				1,850,000	18	
				1,800,000	29	
				1,800,000	32	
				1,900,000	32	

Table S5. List of data points and references for Fig. S13 (continued).

Printing Method	Symbol Shape	Materials	Symbol color	Young's modulus (kPa)	Tensile strain (%)	Reference number
Powder bed fusion (PBF)	Hexagram (✡)	Polyester	Green	14,300	60.5	Ryse et al.[35]
				9,700	1.3	
				11,300	36.1	
				5,900	7.5	

Movie S1. DIW printing a honeycomb structure.

Movie S2. DIW printing a cubic gyroid structure.

Movie S3. Cyclic compression test of a printed cubic gyroid.

^{1}H NMR spectra

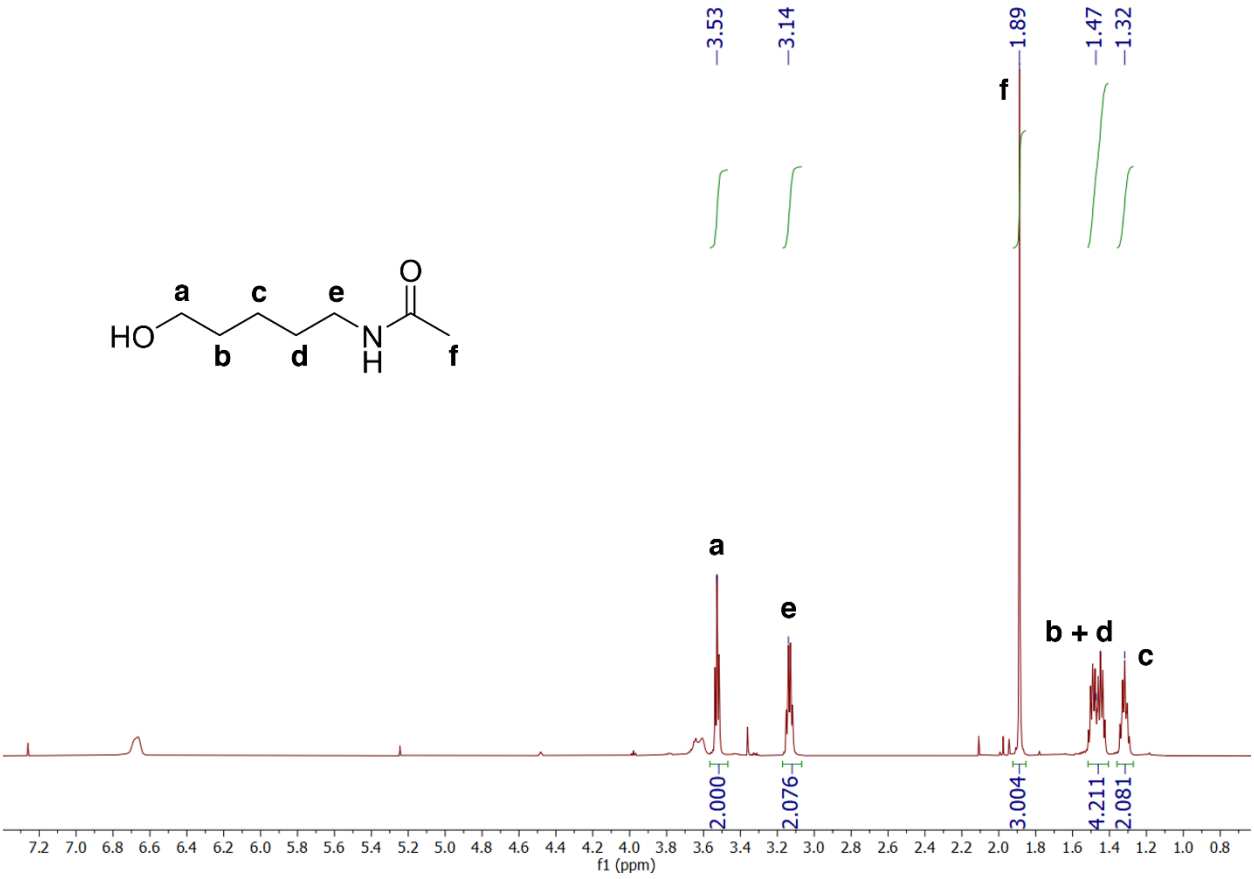

^{1}H NMR of 5-acetamino-1-pentanol.

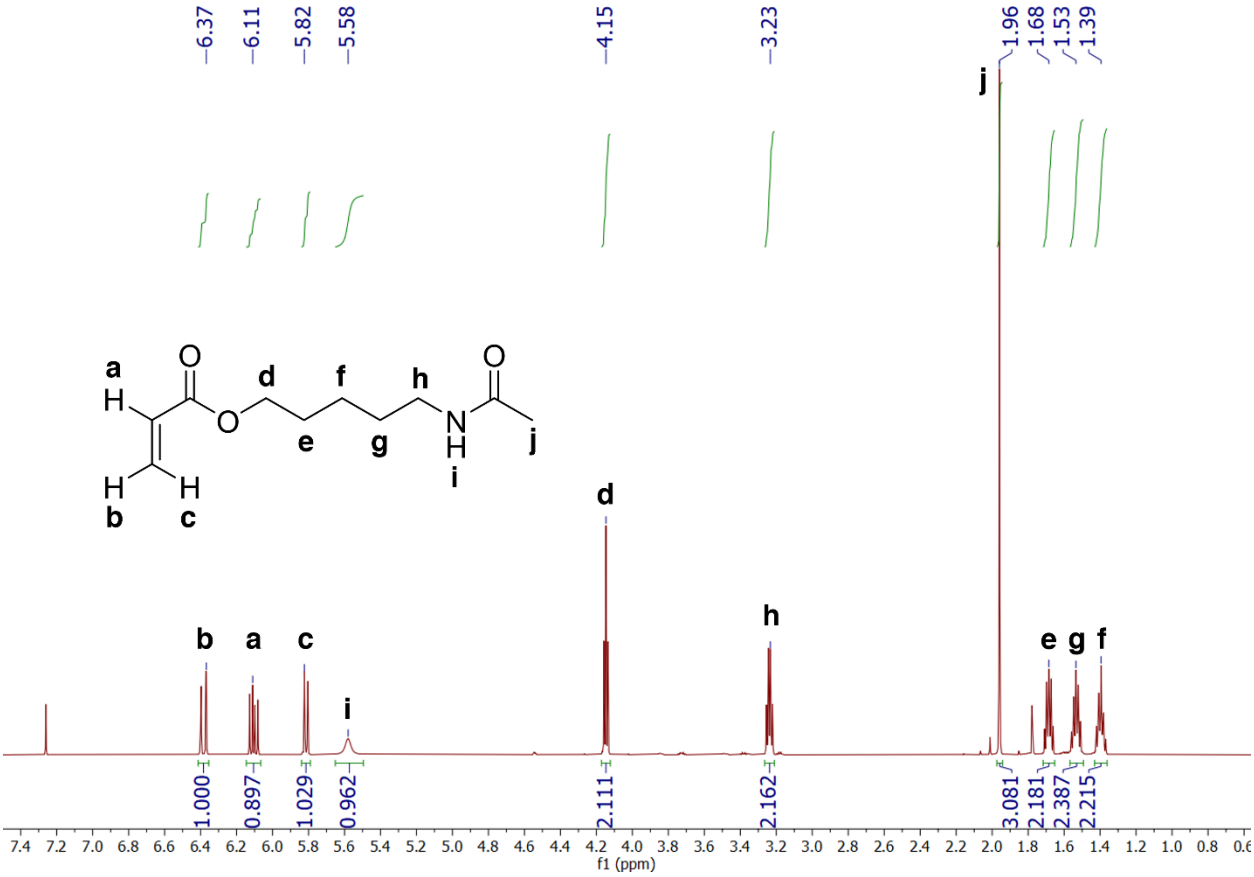

^{1}H NMR of 5-acetaminopentyl acrylate.

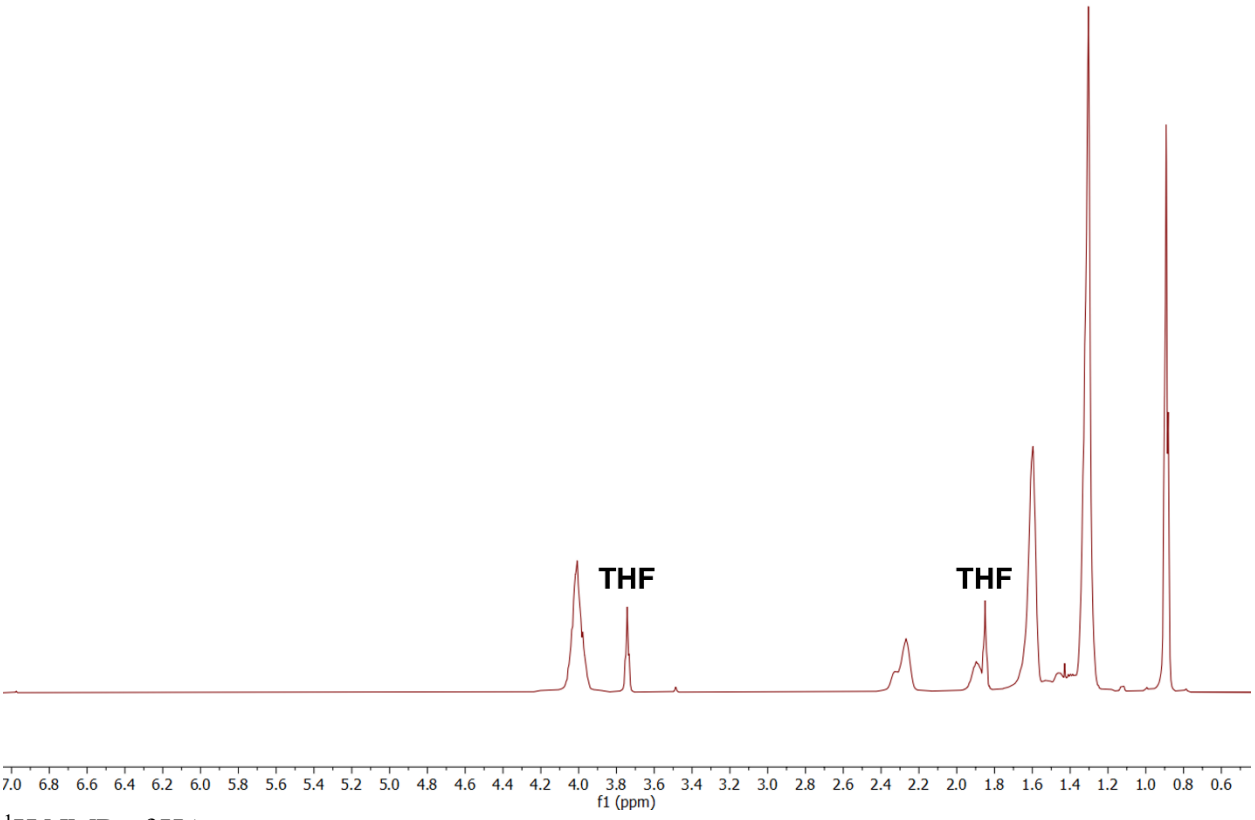

^{1}H NMR of HA_{251}.

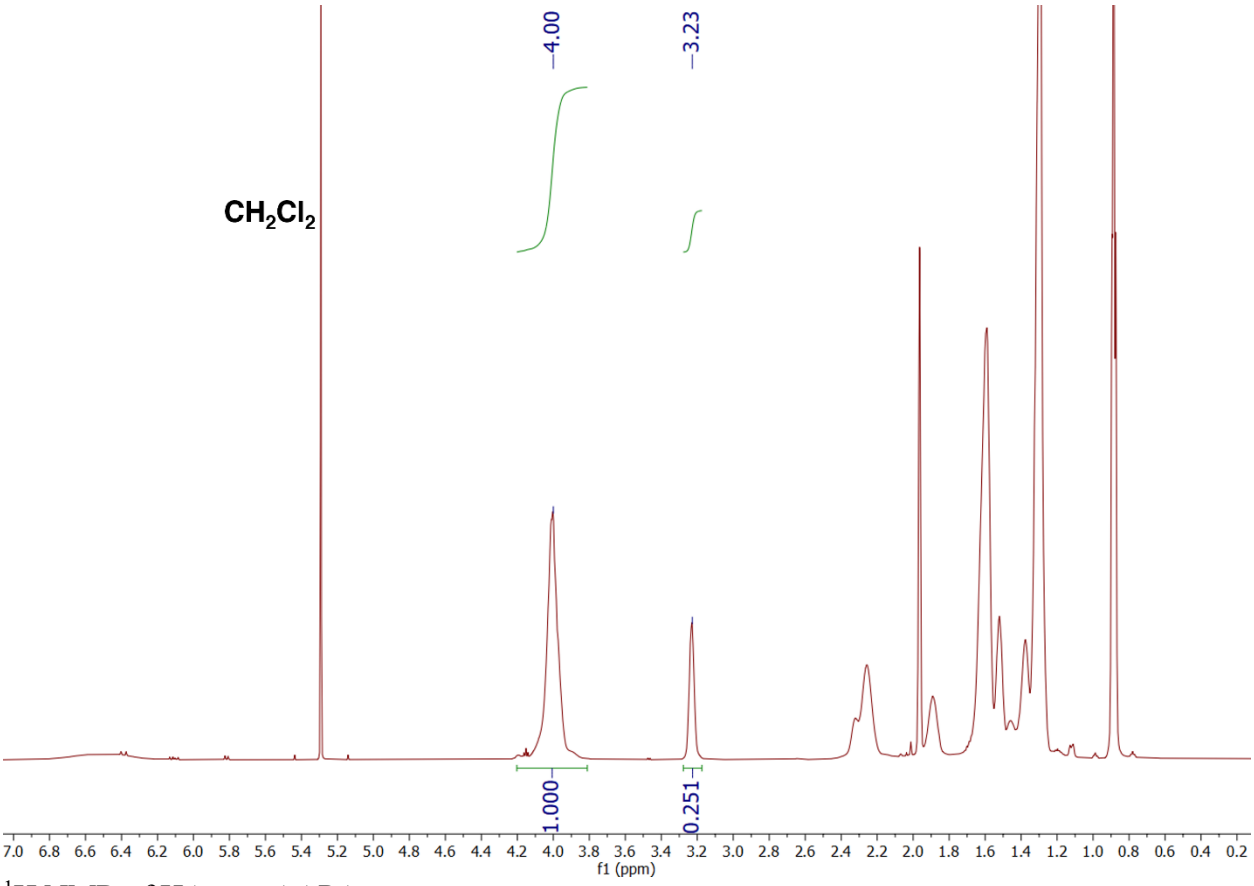

^{1}H NMR of HA_{180}-*r*-$AAPA_{60}$.

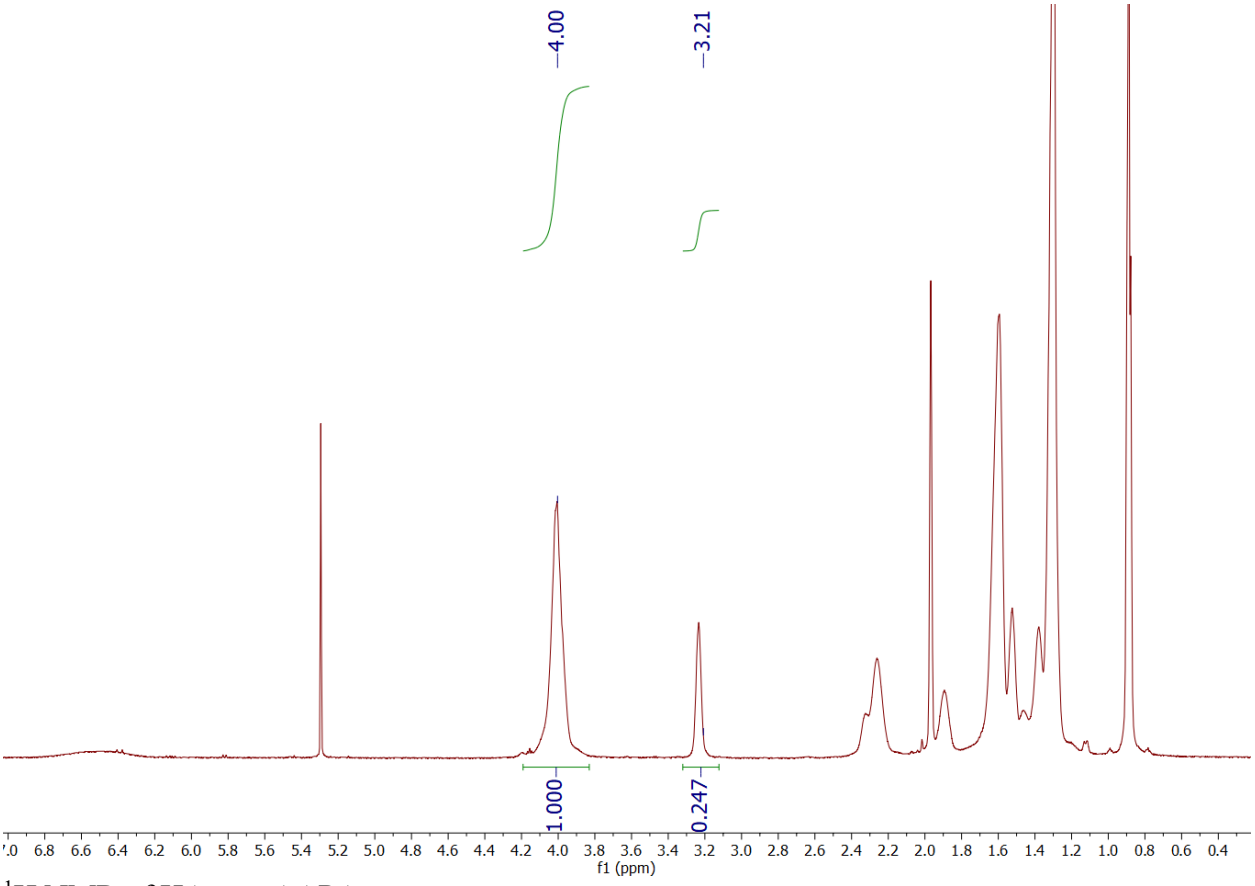

^{1}H NMR of HA_{188}-*r*-$AAPA_{62}$.

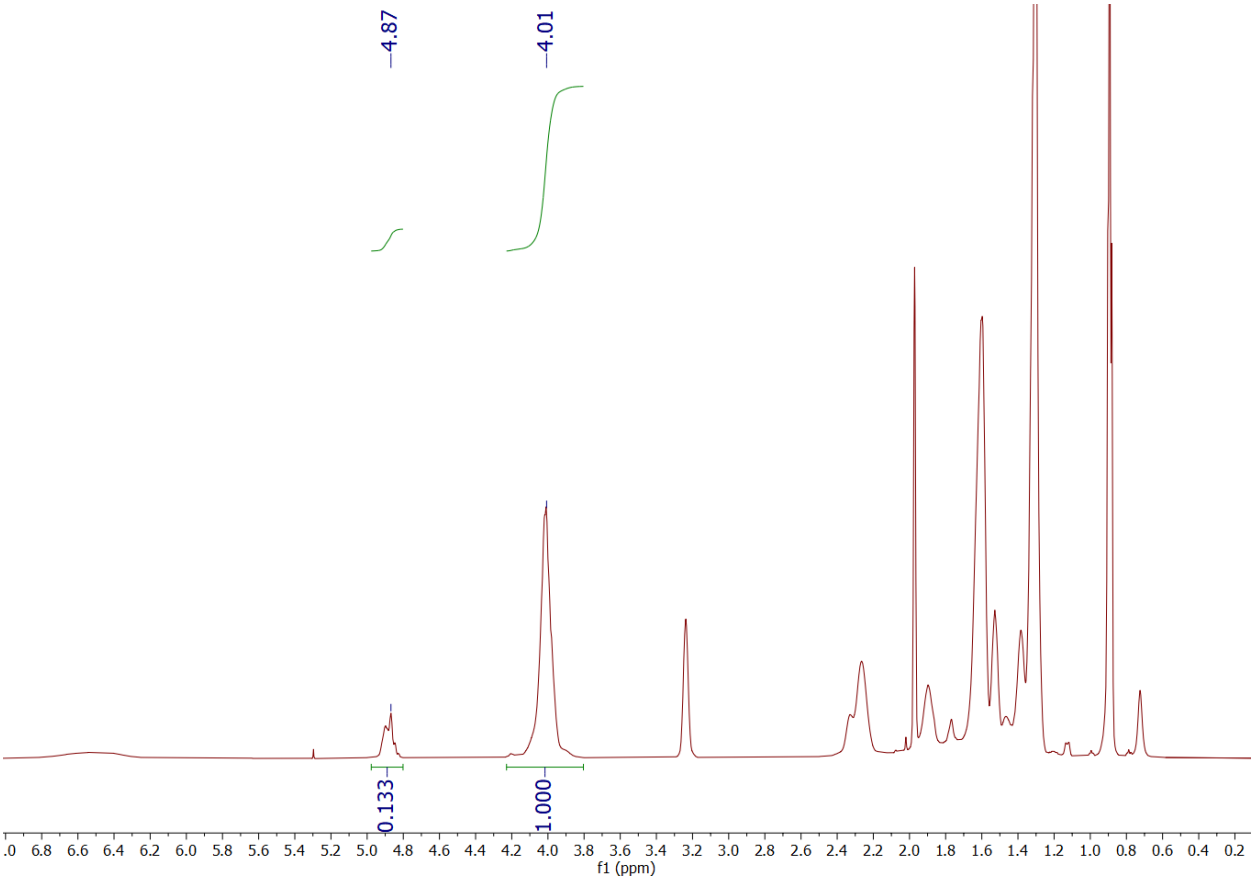

^{1}H NMR of sample TR3, $BnMA_{16}$-*b*-(HA_{180}-*r*-$AAPA_{60}$)-*b*-$PBnMA_{16}$.

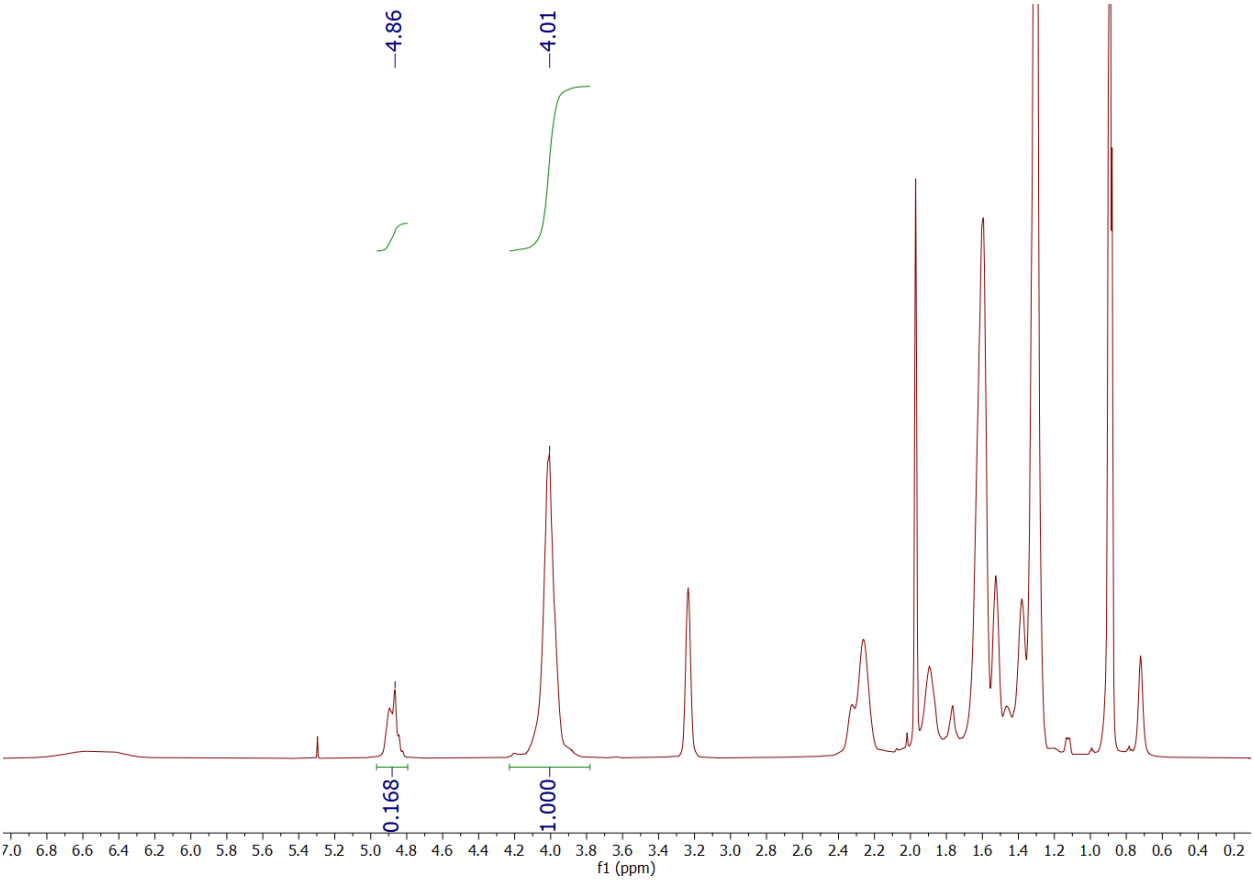

^{1}H NMR of sample TV1, BnMA$_{20}$-*b*-(HA$_{180}$-*r*-AAPA$_{60}$)-*b*-PBnMA$_{20}$.

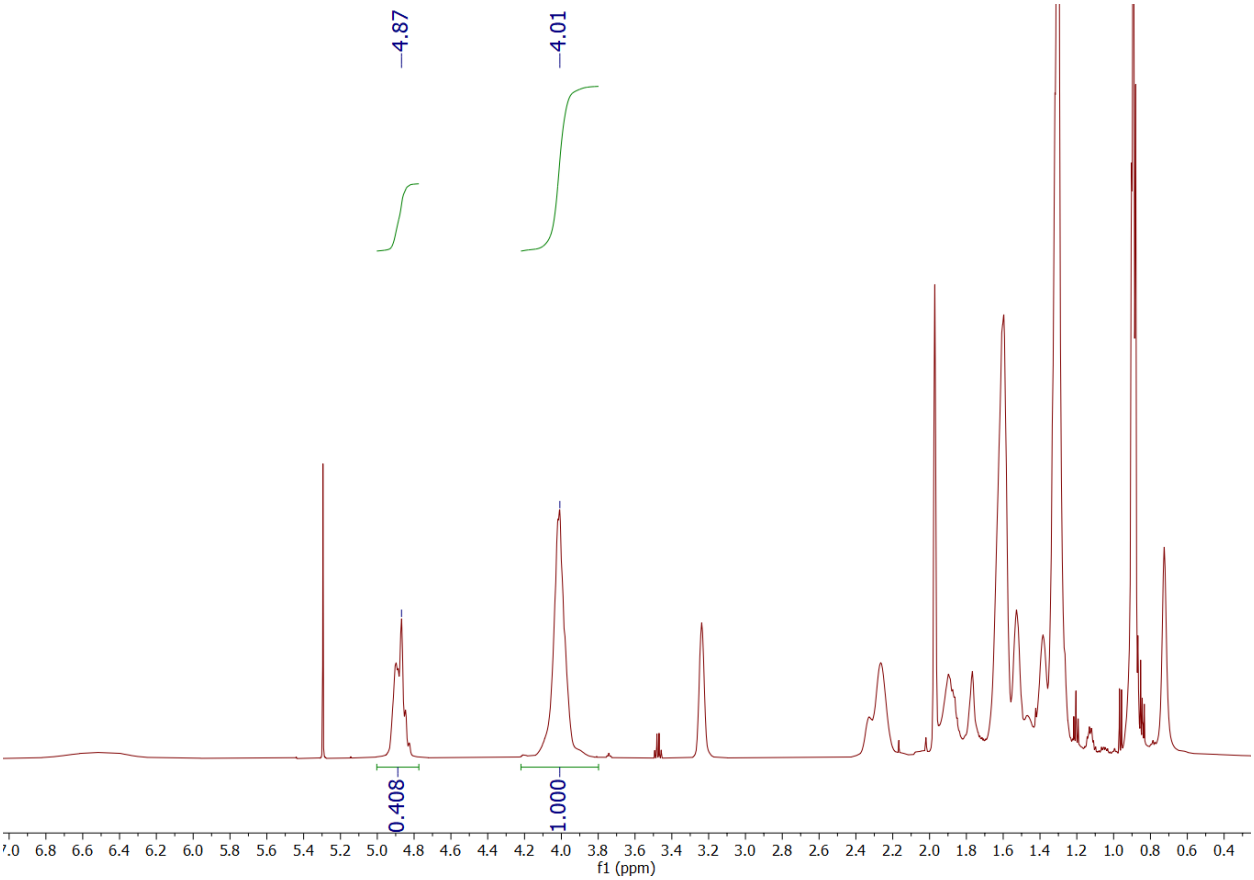

^{1}H NMR of sample TV2, BnMA$_{51}$-*b*-(HA$_{188}$-*r*-AAPA$_{62}$)-*b*-PBnMA$_{51}$.

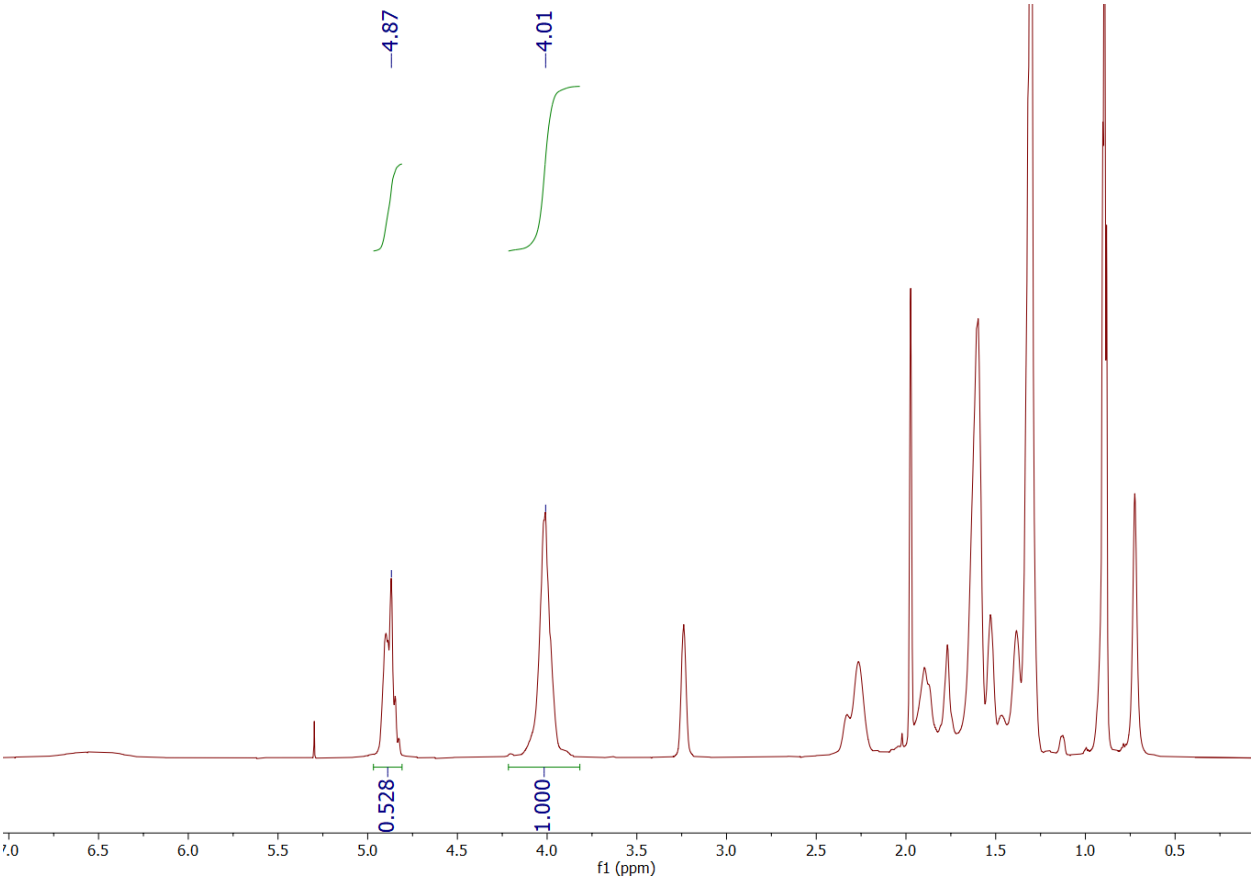

^{1}H NMR of sample TV3, BnMA$_{66}$-*b*-(HA$_{188}$-*r*-AAPA$_{62}$)-*b*-PBnMA$_{66}$.

References

(1) Matyjaszewski, K.; Jakubowski, W.; Min, K.; Tang, W.; Huang, J.; Braunecker, W. A.; Tsarevsky, N. V. Diminishing Catalyst Concentration in Atom Transfer Radical Polymerization with Reducing Agents. *Proc. Natl. Acad. Sci. U. S. A.* **2006**, *103* (42), 15309–15314. https://doi.org/10.1073/pnas.0602675103.

(2) Zhao, B.; Xu, S.; Zheng, S. Synthesis, Self-Assembly and Self-Healing Properties of Organic–Inorganic ABA Triblock Copolymers with Poly(POSS Acrylate) Endblocks. *Polym. Chem.* **2019**, *10* (19), 2424–2435. https://doi.org/10.1039/C9PY00094A.

(3) Chen, Y. L.; Kushner, A. M.; Williams, G. A.; Guan, Z. B. Multiphase Design of Autonomic Self-Healing Thermoplastic Elastomers. *Nat. Chem.* **2012**, *4* (6), 467–472. https://doi.org/10.1038/nchem.1314.

(4) Yirmibesoglu, O. D.; Simonsen, L. E.; Manson, R.; Davidson, J.; Healy, K.; Menguc, Y.; Wallin, T. Multi-Material Direct Ink Writing of Photocurable Elastomeric Foams. *Commun. Mater.* **2021**, *2* (1), 82. https://doi.org/10.1038/s43246-021-00186-3.

(5) Su, S.; He, T.; Yang, H. 3D Printed Multilayer Dielectric Elastomer Actuators. *Smart Mater. Struct.* **2023**, *32* (3), 35021. https://doi.org/10.1088/1361-665X/acb677.

(6) Xie, R.; Mukherjee, S.; Levi, A. E.; Reynolds, V. G.; Wang, H.; Chabinyc, M. L.; Bates, C. M. Room Temperature 3D Printing of Super-Soft and Solvent-Free Elastomers. *Sci. Adv.* **2020**, *6* (46), eabc6900. https://doi.org/10.1126/sciadv.abc6900.

(7) Volpe, R. H.; Mistry, D.; Patel, V. V; Patel, R. R.; Yakacki, C. M. Dynamically Crystalizing Liquid-Crystal Elastomers for an Expandable Endplate-Conforming Interbody Fusion Cage. *Adv. Healthc. Mater.* **2020**, *9* (1), 1901136. https://doi.org/https://doi.org/10.1002/adhm.201901136.

(8) Kim, K.; Guo, Y.; Bae, J.; Choi, S.; Song, H. Y.; Park, S.; Hyun, K.; Ahn, S. K. 4D Printing of Hygroscopic Liquid Crystal Elastomer Actuators. *Small* **2021**, *17* (23), 1–10. https://doi.org/10.1002/smll.202100910.

(9) Wang, Z.; Wang, Z.; Zheng, Y.; He, Q.; Wang, Y.; Cai, S. Three-Dimensional Printing of Functionally Graded Liquid Crystal Elastomer. *Sci. Adv.* **2020**, *6* (39). https://doi.org/10.1126/sciadv.abc0034.

(10) Ambulo, C. P.; Burroughs, J. J.; Boothby, J. M.; Kim, H.; Shankar, M. R.; Ware, T. H. Four-Dimensional Printing of Liquid Crystal Elastomers. *ACS Appl. Mater. Interfaces* **2017**, *9* (42), 37332–37339. https://doi.org/10.1021/acsami.7b11851.

(11) Davidson, E. C.; Kotikian, A.; Li, S.; Aizenberg, J.; Lewis, J. A. 3D Printable and Reconfigurable Liquid Crystal Elastomers with Light-Induced Shape Memory via Dynamic Bond Exchange. *Adv. Mater.* **2020**, *32* (1), 1905682. https://doi.org/10.1002/adma.201905682.

(12) Zhou, L.; Gao, Q.; Fu, J.; Chen, Q.; Zhu, J.; Sun, Y. Multimaterial 3D Printing of Highly Stretchable Silicone Elastomers. *ACS Appl. Mater. Interfaces* **2019**, *11* (26), 23573–23583. https://doi.org/10.1021/acsami.9b04873.

(13) Ford, M. J.; Loeb, C. K.; Pérez, L. X. P.; Gammon, S.; Guzorek, S.; Gemeda, H. B.; Golobic, A. M.; Honnell, A.; Erspamer, J.; Duoss, E. B.; Wilson, T. S.; Lenhardt, J. M. 3D Printing of Transparent Silicone Elastomers. *Adv. Mater. Technol.* **2022**, *7* (5), 2100974. https://doi.org/https://doi.org/10.1002/admt.202100974.

(14) Durban, M. M.; Lenhardt, J. M.; Wu, A. S.; Iv, W. S.; Bryson, T. M.; Perez-perez, L.; Nguyen, D. T.; Gammon, S.; Smay, J. E.; Duoss, E. B.; Lewicki, J. P.; Wilson, T. S. Custom 3D Printable Silicones with Tunable Stiffness. *Macromol. Rapid Commun.* **2018**, *39* (4),

1700563. https://doi.org/10.1002/marc.201700563.
(15) Zheng, R.; Chen, Y.; Chi, H.; Qiu, H.; Xue, H.; Bai, H. 3D Printing of a Polydimethylsiloxane/Polytetrafluoroethylene Composite Elastomer and Its Application in a Triboelectric Nanogenerator. *ACS Appl. Mater. Interfaces* **2020**, *12* (51), 57441–57449. https://doi.org/10.1021/acsami.0c18201.
(16) Kotikian, A.; Truby, R. L.; Boley, J. W.; White, T. J.; Lewis, J. A. 3D Printing of Liquid Crystal Elastomeric Actuators with Spatially Programed Nematic Order. *Adv. Mater.* **2018**, *30* (10), 1–6. https://doi.org/10.1002/adma.201706164.
(17) Brooks, S.; Cartwright, Z.; Merckle, D.; Weems, A. C. 4D Aliphatic Photopolymer Polycarbonates as Direct Ink Writing of Biodegradable, Conductive Graphite-Composite Materials. *Polym. Compos.* **2021**, *42* (10), 5134–5143. https://doi.org/https://doi.org/10.1002/pc.26211.
(18) Liu, W.; Peeke, L. M.; Periyasamy, M.; Campbell, R. R.; Hickner, M. A. Additive Manufacturing of Silicone Composite Structures with Continuous Carbon Fiber Reinforcement. *Polym. Eng. Sci.* **2023**, *63* (6), 1716–1724. https://doi.org/https://doi.org/10.1002/pen.26318.
(19) Chen, K.; Zhang, L.; Kuang, X.; Li, V.; Lei, M.; Kang, G.; Wang, Z. L.; Qi, H. J. Dynamic Photomask-Assisted Direct Ink Writing Multimaterial for Multilevel Triboelectric Nanogenerator. *Adv. Funct. Mater.* **2019**, *29* (33), 1903568. https://doi.org/10.1002/adfm.201903568.
(20) Georgopoulou, A.; Sebastian, T.; Clemens, F. Thermoplastic Elastomer Composite Filaments for Strain Sensing Applications Extruded with a Fused Deposition Modelling 3D Printer. *Flex. Print. Electron.* **2020**, *5* (3), 35002. https://doi.org/10.1088/2058-8585/ab9a22.
(21) Shin, E. J.; Jung, Y. S.; Choi, H. Y.; Lee, S. Synthesis and Fabrication of Biobased Thermoplastic Polyurethane Filament for FDM 3D Printing. *J. Appl. Polym. Sci.* **2022**, *139* (40), e52959. https://doi.org/https://doi.org/10.1002/app.52959.
(22) Shin, E. J.; Park, Y.; Jung, Y. S.; Choi, H. Y.; Lee, S. Fabrication and Characteristics of Flexible Thermoplastic Polyurethane Filament for Fused Deposition Modeling Three-Dimensional Printing. *Polym. Eng. Sci.* **2022**, *62* (9), 2947–2957. https://doi.org/https://doi.org/10.1002/pen.26075.
(23) Georgopoulou, A.; Egloff, L.; Vanderborght, B.; Clemens, F. A Sensorized Soft Pneumatic Actuator Fabricated with Extrusion-Based Additive Manufacturing. *Actuators*. 2021. https://doi.org/10.3390/act10050102.
(24) Khondoker, M. A. H.; Sameoto, D. Direct Coupling of Fixed Screw Extruders Using Flexible Heated Hoses for FDM Printing of Extremely Soft Thermoplastic Elastomers. *Prog. Addit. Manuf.* **2019**, *4* (3), 197–209. https://doi.org/10.1007/s40964-019-00088-4.
(25) Wang, J.; Zhang, Y.; Sun, W.; Chu, S.; Chen, T.; Sun, A.; Guo, J.; Xu, G. Morphology Evolutions and Mechanical Properties of In Situ Fibrillar Polylactic Acid/Thermoplastic Polyurethane Blends Fabricated by Fused Deposition Modeling. *Macromol. Mater. Eng.* **2019**, *304* (7), 1900107. https://doi.org/https://doi.org/10.1002/mame.201900107.
(26) Schimpf, V.; Max, J. B.; Stolz, B.; Heck, B.; Mülhaupt, R. Semicrystalline Non-Isocyanate Polyhydroxyurethanes as Thermoplastics and Thermoplastic Elastomers and Their Use in 3D Printing by Fused Filament Fabrication. *Macromolecules* **2019**, *52* (1), 320–331. https://doi.org/10.1021/acs.macromol.8b01908.
(27) Joe, J.; Shin, J.; Choi, Y.-S.; Hwang, J. H.; Kim, S. H.; Han, J.; Park, B.; Lee, W.; Park, S.;

Kim, Y. S.; Kim, D.-G. A 4D Printable Shape Memory Vitrimer with Repairability and Recyclability through Network Architecture Tailoring from Commercial Poly(ε-Caprolactone). *Adv. Sci.* **2021**, *8* (24), 2103682. https://doi.org/https://doi.org/10.1002/advs.202103682.

(28) Niu, W.; Zhang, Z.; Chen, Q.; Cao, P.-F.; Advincula, R. C. Highly Recyclable, Mechanically Isotropic and Healable 3D-Printed Elastomers via Polyurea Vitrimers. *ACS Mater. Lett.* **2021**, *3* (8), 1095–1103. https://doi.org/10.1021/acsmaterialslett.1c00132.

(29) Kumar, N.; Jain, P. K.; Tandon, P.; Pandey, P. M. The Effect of Process Parameters on Tensile Behavior of 3D Printed Flexible Parts of Ethylene Vinyl Acetate (EVA). *J. Manuf. Process.* **2018**, *35*, 317–326. https://doi.org/10.1016/j.jmapro.2018.08.013.

(30) Ravichandran, D.; Kakarla, M.; Xu, W.; Jambhulkar, S.; Zhu, Y.; Bawareth, M.; Fonseca, N.; Patil, D.; Song, K. 3D-Printed in-Line and out-of-Plane Layers with Stimuli-Responsive Intelligence. *Compos. Part B Eng.* **2022**, *247*, 110352. https://doi.org/https://doi.org/10.1016/j.compositesb.2022.110352.

(31) Ravichandran, D.; Ahmed, R. J.; Banerjee, R.; Ilami, M.; Marvi, H.; Miquelard-Garnier, G.; Golan, Y.; Song, K. Multi-Material 3D Printing-Enabled Multilayers for Smart Actuation via Magnetic and Thermal Stimuli. *J. Mater. Chem. C* **2022**, *10* (37), 13762–13770. https://doi.org/10.1039/D2TC01109C.

(32) Hupfeld, T.; Wegner, A.; Blanke, M.; Doñate-Buendía, C.; Sharov, V.; Nieskens, S.; Piechotta, M.; Giese, M.; Barcikowski, S.; Gökce, B. Plasmonic Seasoning: Giving Color to Desktop Laser 3D Printed Polymers by Highly Dispersed Nanoparticles. *Adv. Opt. Mater.* **2020**, *8* (15), 2000473. https://doi.org/https://doi.org/10.1002/adom.202000473.

(33) Do, N. B.; Imenes, K.; Aasmundtveit, K. E.; Nguyen, H.-V.; Andreassen, E. Thermal Conductivity and Mechanical Properties of Polymer Composites with Hexagonal Boron Nitride—A Comparison of Three Processing Methods: Injection Moulding, Powder Bed Fusion and Casting. *Polymers*. 2023. https://doi.org/10.3390/polym15061552.

(34) Chen, A. Y.; Chen, A.; Wright, J.; Fitzhugh, A.; Hartman, A.; Zeng, J.; Gu, G. X. Effect of Build Parameters on the Mechanical Behavior of Polymeric Materials Produced by Multijet Fusion. *Adv. Eng. Mater.* **2022**, *24* (9), 2100974. https://doi.org/https://doi.org/10.1002/adem.202100974.

(35) Vande Ryse, R.; Edeleva, M.; Van Stichel, O.; D'hooge, D. R.; Pille, F.; Fiorio, R.; De Baets, P.; Cardon, L. Setting the Optimal Laser Power for Sustainable Powder Bed Fusion Processing of Elastomeric Polyesters: A Combined Experimental and Theoretical Study. *Materials*. 2022. https://doi.org/10.3390/ma15010385.